Full title: Loss of pseudouridine synthases in the RluA family causes hypersensitive nociception in *Drosophila*

Short title: Pseudouridine synthase RluA in nociception

Wan Song[1,2] & W. Daniel Tracey[1,2,*]

[1]Gill Center for Biomolecular Research, Indiana University, Bloomington, Indiana, USA

[2]Department of Biology, Indiana University, Bloomington, Indiana, USA

[*] Corresponding author

Email: dtracey@indiana.edu

Abstract

Nociceptive neurons of *Drosophila* larvae are characterized by highly branched dendritic processes whose proper morphogenesis relies on a large number of RNA-binding proteins. Post-transcriptional regulation of RNA in these dendrites has been found to play an important role in their function. Here, we investigate the neuronal functions of two putative RNA modification genes, *RluA-1* and *RluA-2*, which are predicted to encode pseudouridine synthases. *RluA-1* is specifically expressed in larval sensory neurons while *RluA-2* expression is ubiquitous. Nociceptor-specific RNAi knockdown of *RluA-1* caused hypersensitive nociception phenotypes, which were recapitulated with genetic null alleles. These were rescued with genomic duplication and nociceptor-specific expression of *UAS-RluA-1-cDNA*. As with *RluA-1*, *RluA-2* loss of function mutants also displayed hyperalgesia. Interestingly, nociceptor neuron dendrites showed a hyperbranched morphology in the *RluA-1* mutants. The latter may be a cause or a consequence of heightened sensitivity in mutant nociception behaviors.

Author Summary

Pseudouridine (Psi) is a C5-glycoside isomer of uridine and it is the most common posttranscriptional modification of RNAs, including noncoding tRNAs, rRNAs, snRNAs as well as mRNAs. Although first discovered in the 1950s, the biological functions of Psi in multicellular organisms are not well understood. Interestingly, a marker for sensory neurons in *Drosophila* encodes for a putative pseudouridine synthase of unknown function called RluA-1. Here, we report our characterization of nociception phenotypes for larvae with RluA-1 loss of function along with that of a related gene RluA-2. Disrupting either or both RluA-1 and RluA-2 resulted in hypersensitive nociception. In addition, RluA-1 mutants have more highly branched nociceptor neurites that innervate the epidermis. Our studies suggest an important role for the

RluA family in nociception. This may be through its action on RNAs that regulate neuronal excitability and/or dendrite morphogenesis.

Introduction

Pain serves an indispensable, protective role but when pain becomes pathological it can have a debilitating impact on human life. The total annual cost of pain to society in the United States was estimated by the Institute of Medicine to be up to $635 billion, which is greater than that of heart disease, cancer, and diabetes combined (1). It is therefore of urgent importance to uncover the basic molecular and cellular mechanisms involved in pain in order to better treat it. Laboratory animal models of pain and nociception have played an essential role in identifying such mechanisms. *Drosophila* larvae respond to noxious thermal and mechanical stimuli through stereotyped rolling escape locomotion (in which the larva rotates around its long body axis), which is robust and easily distinguishable from other forms of locomotion (2). Rolling is used as a behavioral defense against attacks by parasitoid wasps which lay their eggs within the fly larvae using a sharp ovipositor (3). Successful wasp infection is lethal to the larvae and is a strong selective pressure in natural populations of *Drosophila.* Combined with the unparalleled genetic tools available for *Drosophila melanogaster*, this behavioral readout provides an excellent system to study the genetics of nociception and pain (2, 4-8). Previous studies have demonstrated a specific subset of dendritic arborization (da) sensory neurons in the peripheral nervous system, Class IV multidendritic da (clVda) neurons, are of critical importance for thermal, mechanical and high intensity light nociception (3, 9, 10). Further evidence suggests a lesser but significant contribution of Class II (cIIda) and Class III da (cIIIda) neurons in mechanical nociception (3, 11). In addition, great progress has been made in identifying the circuits in the larval abdominal ganglion that are involved in rolling escape locomotion (12-15).

Genes that are specifically expressed in multidendritic (md) neurons have been found to play a role in nociception. For instance, *painless* (2) is required for mechanical and thermal nociception and it is expressed in all four classes of md neurons. Mechanical nociception genes such as *pickpocket* (16), *ppk26/balboa* (17, 18) and the polymodal nociception gene *dTRPA1-C/D* (19) each show very specific expression in the cIVda neurons. Forward genetic screens have also identified a set of genes with enriched expression in the cIVda neurons which either inhibit or activate nociceptive pathways (20).

The historically first known genetic marker with specific expression pattern in the da neurons was the *lacZ* enhancer trap *E7-2-36* (21). Later studies reported that this enhancer trap gene was inserted upstream of the *RluA-1* gene and DNA sequences from upstream of *RluA-1* caused expression of GAL4 in multidendritic neurons (22). The *RluA1* gene encodes an enzyme that is predicted to have pseudouridine synthase activity, but how this RNA modifying protein is involved in the function of nociceptive multidendritic neurons remains unknown.

A widespread importance of RNA-binding proteins in cIVda neuron dendrite morphogenesis and function was found in a recent large-scale RNAi screen that identified 88 genes encoding RNA-binding proteins whose knockdown caused aberrant dendrite morphogenesis (23). The elaborate dendrite arbors of cIVda neurons project long distances from the neuronal cell body and mRNA granules are trafficked to these distant sites where they may undergo local translation. Indeed, RNA granules containing Nanos (Nos), Pumilio (Pum), Oskar (Osk), Fragile X Mental Retardation (FMRP) and other proteins have been shown to regulate the formation of higher order dendrites in these cells (24-28). Interestingly, the *nos* mRNA itself is transported into dendrites via a pathway that relies on Oskar and Rumplestiltskin, two proteins that also play a role regulating *nos* in the early embryo (28).

Mechanical nociception defects are also observed in animals with disruption in these pathways (28).

Pseudouridylation is the most common post-transcriptional RNA modification. Pseudouridine (Ψ), the C5-glycoside isomer of uridine, was initially found in many positions in rRNA, tRNA and snRNA in all organisms that have been investigated (29). RNA-seq based global pseudouridine profiling has shown the presence of Ψ in many mRNAs and a large number of those sites were found to be dynamically regulated in yeast and human cells (30-33). Dysfunctional pseudouridylation has been linked to several human diseases (34-36). Since many sites of pseudouridylation in different organisms are evolutionarily conserved, *Drosophila melanogaster* may provide an excellent and genetically tractable metazoan system to elucidate some of these functions.

The isomerization of uridine to pseudouridine is catalyzed by six families of pseudouridine synthases. They function either as guide RNA directed ribonucleoprotein complexes or as stand-alone proteins (37, 38). In the *Drosophila* genome, 9 proteins have been identified with annotated pseudouridine synthase domains. Minifly (mfl), the RNA-dependent pseudouridine synthase homolog of human dyskerin (mouse NAP57 and yeast Cbf5), is required for somatic stem cell homeostasis and is essential for *Drosophila* viability and fertility (39-41). Knockout of *Drosophila* Pus7, the human and yeast Pus7 homolog, results in increased aggressiveness in adult flies (36). The function and specificity of other predicted pseudouridine synthases are largely unknown. Among the six families, the RluA family, which does not rely on guide RNAs, appears to be the most complex based on divergent substrate specificities in bacteria and yeast (42). RluA family members in bacteria are involved in ribosomal assembly and growth (43, 44) but their function in multicellular organisms has not been studied. Although pseudouridine synthases appear to function ubiquitously, as noted above, *Drosophila RluA-1*, a

109 member in RluA family, has been reported to be specifically expressed in md neurons (22). Thus,
110 we have investigated the role for *RluA-1* and its paralog *RluA-2*, in nociception pathways that
111 are known to depend on md neurons. Our results indicate an important function for *RluA-1* and
112 *RluA-2* in the regulation of nociception.

113 ## Results

114 ### *RluA-1* is expressed in the multidendritic neurons of the peripheral nervous system
115 ### and in the cells of brain

116 Previously described reporter genes for *RluA-1* showed specific expression in larval
117 multidendritic neurons (22). We replicated this finding by generating an *RluA-1*^{GAL4} driver at the
118 endogenous gene locus through recombination mediated cassette exchange (RMCE) of *RluA-*
119 *1*^{MI06897} (an intronic MiMIC) and a Trojan exon cassette (45). An mCD8GFP reporter driven by
120 *RluA-1*^{GAL4} was expressed in peripheral sensory neurons in each segment of the larval body wall
121 (**Fig 1A**). In the dorsal cluster, GFP-positive signals were clearly detected in all four classes of
122 md-da sensory neurons, dorsal multiple dendrite neuron (dmd1), external sensory (ES) and
123 dorsal bipolar dendritic (dbd) neurons (**Fig 1B**). In the larval ventral nerve cord, the GFP-positive
124 signals were seen in the axonal projections of the sensory neurons (**Fig 1C**). GFP signal was also
125 observed in the unidentified clusters of neurons in the larval brain (**Fig 1C).** In the adult brain,
126 significant signals were detected in the optic lobes and other small cell clusters of the central
127 brain (**S1A Fig**).

128 To determine the localization of the RluA-1 proteins, we generated a GFSTF exon trap
129 (46) that expresses an in frame GFP fusion with *RluA-1* at the endogenous genomic locus (with
130 RMCE of the *RluA-1*^{MI06897} MiMIC element) (46). Although live imaging did not detect the EGFP
131 tagged RluA-1 protein, immunostaining with anti-GFP labelled nuclei of larval multidendritic
132 neurons, ES and dbd neurons also expressing a membrane-localized RFP (*Gal4109(2)80* > *UAS-*

133 *CD8-RFP*, **Fig 1D**). The tagged RluA-1 protein was also detected in the cell bodies of neurons in
134 optic lobes and other yet-to-be identified cells in the adult brain (**S1B Fig**).

135 Reducing or removing *RluA-1* results in a hypersensitive thermal nociception 136 phenotype

137 Given our confirmation of the expression of the *RluA1* gene and protein in the
138 multidendritic neurons we tested for potential roles of RluA-1 in the regulation of nociception.
139 To do so, we first performed tissue-specific knockdown using GAL4/UAS based RNA
140 interference (RNAi). A cIVda specific driver (*ppk1.9-GAL4 UAS-dicer2*) (47) was employed to
141 drive an *RluA-1* RNAi construct in the larval cIVda nociceptors. We assessed potential
142 insensitive phenotypes (with a probe temperature of 46°C) and potential hypersensitive
143 phenotypes (with a temperature of 42°C) as previously described (20). When stimulated with
144 the higher temperature 46°C probe the *RluA-1-RNAi* larvae responded significantly faster than
145 the *ppk-GAL4* driver alone controls. This genotype also responded faster than the UAS-RNAi
146 controls but this difference was not statistically significant (**Fig 2A**). The results suggested that
147 reducing *RluA-1* in classIV neurons may have made the larvae more sensitive to noxious heat.
148 Indeed, a clearly hypersensitive phenotype for the *RluA1*-RNAi animals was seen when testing
149 with 42°C probe (**Fig 2A**). The average latency to roll in the *RluA-1* knock-down animals was
150 significantly faster than the driver alone animals or the *UAS-RNAi* control animals. These data
151 combined suggest that reducing the activity of *RluA-1* in the noxious heat-responsive cIVda
152 cells caused thermal hyperalgesia.

153 To further test the function of *RluA-1* we next generated a precise genetic deletion
154 mutant of *RluA-1* in which 11.14 kbp including the entire *RluA-1* genomic region was removed
155 by CRISPR-guided homologous recombination-directed repair (HDR) (48). Homology arms of
156 ~1kb immediately flanking the CRIPSPR cleavage sites were used to direct the HDR (**S2A Fig**).

157 The resultant deletion mutant (*RluA-1*$^{del\text{-}HDR}$) was confirmed by PCR amplification and
158 sequencing of PCR products from the targeted *RluA-1* locus (**S2B Fig**). To facilitate the
159 behavioral comparisons, the *RluA-1*$^{del\text{-}HDR}$ mutant was backcrossed six times to our most
160 commonly used genetic background strains Canton-S (CS), w^{1118}, and isogenized w^{1118} (isow^{1118}).
161 As with class IV md neuron-specific RNAi knockdown, *RluA-1*$^{del\text{-}HDR}$ larvae showed significantly
162 faster responses to noxious heat stimulation of 42°C compared to the corresponding control
163 animals, regardless of genetic background (**Fig 2B**). Note that for unknown reasons, these
164 genetic backgrounds vary in their baseline responses. This genetic background effect has a
165 significant impact on the latency of larval nociception responses to noxious heat stimuli, with
166 the most striking differences between homozygous *RluA-1*$^{-/-}$ and the relatively insensitive
167 isow^{1118} background, followed by that of w^{1118} background, and then the CS background (**Fig**
168 **2B**).

169 Given the sensitivity to genetic background, we performed an additional genetic test
170 for the importance of *RluA-1*, by generating an independent mutant allele
171 (*RluA-1*$^{del\text{-}FRT}$) using FLP recombinase and FRT-bearing insertions (49) (*PBac{WH}*^{f02750}(+) and
172 *p{XP}*^{d2586}(-), **S2A Fig**). Transheterozygous *RluA-1*$^{del\text{-}FRT}$/*RluA-1*$^{del\text{-}HDR}$ mutant larvae displayed
173 hypersensitivity to a 42°C stimulus (**Fig 2C**)) indicating that *RluA-1*$^{del\text{-}FRT}$ failed to complement
174 *RluA-1*$^{del\text{-}HDR}$. Failure of complementation of independently generated alleles created in distinct
175 genetic backgrounds provides strong evidence that the hypersensitive nociceptive phenotypes
176 observed are a consequence of the mutation of *RluA-1* and not due to unlinked mutations
177 present in one background or another.

178 For the remainder of our behavioral studies, we relied on the isogenized w^{1118}
179 background. This had the advantage of greater genetic uniformity relative to w^{1118} and CS, as
180 well as showing the strongest hypersensitive mutant phenotype for *RluA-1*.

181 **Genetic rescue of *RluA-1* mutant restores thermal nociception response**

182 To test that the mutation in *RluA-1* was the underlying cause of the hypersensitive
183 nociception phenotype, we introduced a genomic rescue construct into the *RluA-1*$^{del\text{-}HDR}$ mutant
184 background (a Bacterial Artificial Chromosome (BAC) (P6-D7)) (50) covering the *RluA-1* gene
185 region). With the 42°C stimulus, larvae with two copies of the duplication (Dp) in the
186 background of *RluA-1*$^{del\text{-}HDR}$ showed rescue of the hypersensitivity (**Fig 3A**). This rescue with the
187 genomic duplication was dosage dependent. Larvae with only one copy of the Dp in the *RluA-*
188 *1*$^{del\text{-}HDR}$ background (*RluA-1*$^{-/-}$; *Dp*$^{+/-}$) responded more slowly than the mutant this difference was
189 not statistically significant (**Fig 3A**). Combined, the results of genomic rescue experiments
190 support the hypothesis that mutation of *RluA-1* is indeed the cause of the hypersensitive
191 thermal nociception phenotype.

192 A caveat remained in that the genomic rescue construct included other genes in
193 addition to *RluA-1*. Thus, genomic rescue did not rule out the possibility that a mutation tightly
194 linked to *RluA-1*, but not in *RluA-1* itself, was responsible for the mutant phenotype. Thus, as a
195 final test, we generated transgenic lines to express an *RluA-1* cDNA under the control of the
196 GAL4/UAS system (*UAS-RluA-1*). Using the *UAS-RluA-1* we specifically restored *RluA-1* to cIVda
197 neurons in the *RluA-1* null mutant background. When stimulated with the 42°C probe the
198 animals with both the *ppkGal4* driver and the *UAS-RluA-1-cDNA* transgene in the *RluA-1* $^{del\text{-}HDR}$
199 showed a complete rescue from the hypersensitivity seen in the null mutant (**Fig 3B**). Neither
200 the *ppkGal4* driver alone nor the *UAS-RluA-1* had an effect on the hypersensitive thermal
201 nociception phenotype in the *RluA-1* null mutant background, excluding the possibility of non-
202 specific effects of these transgenes (**Fig 3B**). In addition, overexpression of *UAS-RluA1* with a
203 md neuron driver (MD-Gal4) had no effect on nociception behavior at 42°C stimulus ruling out
204 the possibility that the increased latency seen in the rescue effect was a non-specific

consequence of over-expression (**S3 Fig**). Combined, these nociceptor-specific rescue experiments provide genetic confirmation that loss-of-function mutation in *RluA-1* causes hypersensitive thermal nociception and localizes the site of action for RluA-1 in this process to the nociceptors.

RluA-1 requirement for mechanosensory thresholds

The cIVda neurons are not only required for detection of noxious heat, they also contribute to sensing harsh mechanical stimulation (3, 16, 17). Thus, we investigated the *RluA-1* mutant responses to noxious mechanical stimuli. When stimulated with a 30mN/720kPa Von Frey fiber, significantly more *RluA-1*$^{\text{del-HDR}}$ null mutant larvae performed the typical nociceptive rolling behavior compared to the isow^{1118} controls (**Fig 4A**). Even when the probe strength/pressure was reduced to 15mN/360kPa, the majority of *RluA-1*$^{-/-}$ larvae still rolled while less than half of control larvae rolled (**Fig 4A**), indicating the defect in *RluA-1* also caused hypersensitive mechanical nociception. Loss of *RluA-1* did not have any impact on behavioral responses to gentle touch (**Fig 4B**) suggesting a more specific involvement in nociception than for sensory processing in general.

Expression pattern and nociception functions for RluA-2

The *RluA-2* locus is adjacent to *RluA-1* on the second chromosome of *Drosophila melanogaster*. *RluA-2* has significant sequence similarity with *RluA-1* within the evolutionarily conserved pseudouridine synthase domain. This amino acid similarity of *RluA1* and *RluA2* suggested possible functional overlap for the encoded proteins. To investigate the expression of RluA-2 we generated a GFSTF line with RMCE of the *RluA-2*^{Ml12981} mimic element (**S4A Fig**) (46). Immunostaining with anti-GFP labelled nuclei in all of the cell types that we observed in third instar larvae (**Fig 5A**), including md neurons (**Fig 5B**).

To test the function of *RluA-2* we generated a deletion (*RluA-2*$^{del\text{-}HDR}$) to remove its pseudouridine synthase domain via CRISPR/Cas9 HDR (**S4A Fig**). Also, since RluA-1 and RluA-2 are both expressed in the md neurons (**Fig 1D** and **Fig 5B**), we generated a double mutant (*RluA-1*$^{del\text{-}HDR}$*RluA-2*$^{del\text{-}HDR}$), by injecting the *RluA-2*$^{del\text{-}HDR}$ constructs in the *RluA-1*$^{del\text{-}HDR}$ null mutant background (**S4 Fig**). The double mutant allowed us to completely remove RluA pseudouridine synthase gene activity from the flies. Prior to functional assessment, the single mutant and the double mutant were backcrossed six times to the genetic background of iso*w*^{1118}.

We tested each single mutant (*RluA-1*$^{del\text{-}HDR}$ and *RluA-2*$^{del\text{-}HDR}$) together with the double mutant *RluA-1*$^{del\text{-}HDR}$ *RluA-2*$^{del\text{-}HDR}$ side by side in thermal nociception assays with the 42°C thermal stimulus. *RluA-1*$^{del\text{-}HDR}$ larvae (*RluA-1*$^{-/-}$) again responded significantly faster than the genetic background control (**Fig 6**). The *RluA-2*$^{del\text{-}HDR}$ single mutant larvae also displayed a faster response to the stimulus (**Fig 6**) and similar hypersensitivity was also seen in an independent allele for *RluA-2* that we generated by FLP/FRT mediated recombination (*RluA-2*$^{del\text{-}FRT}$) allele (**S5 Fig**). Finally, the double mutant *RluA-1*$^{del\text{-}HDR}$ *RluA-2*$^{del\text{-}HDR}$ larvae showed a faster response than the control larvae (**Fig 6**) to the same extent as the single mutant of *RluA-2*$^{del\text{-}HDR}$. These results indicated that *RluA-2*, like *RluA-1*, negatively regulates nociception. The finding that the double mutant did not show a more severe phenotype than either single mutant suggests that RluA-2 and RluA-1 have non-redundant functional roles, and that they may function in the same molecular pathway. When this pathway is disrupted, hypersensitive nociception results.

RluA-1 regulates neuronal dendrite morphology of nociceptors

A nociceptor-specific RNAi screen with thermal nociception assay discovered dozens of genes whose reduction caused either insensitive or hypersensitive thermal nociception (20). Interestingly, some of those genes targeted with RNAi showed a reduced or increased

branching of Class IV neuron dendrites. Reduced dendrite branching was often seen with nociceptive insensitivity while increased branching was found in some hypersensitive genotypes. Thus, regulation of Class IV neuron dendrite morphology is a commonly affected developmental pathway that is related to nociception phenotypes. Given this, we investigated the dendrite morphology of the cIVda neuron dendrites in the *RluA-1*$^{del\text{-}HDR}$ mutant. In mutant ddaC neurons visualized with *ppk-CD4-tdTom*ato, we observed a modest but significant increase in the number of dendrite branches (normalized by neuron size) and shorter average branch length in comparison to control animals (**Figs 7A and 7B**). We also found that dendritic branches in the *RluA-1*$^{del\text{-}HDR}$ ddaC neurons had higher frequency of isoneuronal cross-over events compared to the control (**Figs 7C and 7D**). This latter phenotype is suggestive of an isoneuronal tiling defect. Increased isoneuronal crossovers are also seen in mutants that affect dendrite attachment to the basal lamina (51-54). Whether or not these dendrite abnormalities play a causal role in the hypersensitive nociception phenotypes of the *RluA-1* mutant will be an interesting subject for future investigation.

Discussion

Given the well-established nociceptive role of md-neurons, we have investigated the historically first known molecular marker for md-neurons in nociception pathways. This gene encodes the RluA-1 protein in the RluA family of pseudouridine synthases. Our studies clearly demonstrate that loss of function for either *RluA-1* or *RluA-2* produce hyperalgesia in third instar *Drosophila* larvae. Tissue-specific RNAi, genetic null mutant, and cDNA rescue experiments all indicate that loss of the *RluA-1* gene from whole animals, or specifically from nociceptors, results in hyperalgesia. A newly generated *RluA-1*^{GAL4} driver showed specific expression in larval multidendritic and ES neurons. As well, a GFP exon trap for RluA-1 protein localized to the nuclei of these neurons. A small number of unidentified neurons in the larval

brain were also revealed by *RluA-1*^{GAL4} and we observed expression of *RluA-1*^{GAL4} driven mCD8GFP and GFP tagged RluA-1 in cells of the adult brain, which included the optic lobe.

Although loss of *RluA-2* also caused hyperalgesia, its expression pattern was ubiquitous and included multidendritic neurons. Like the RluA-1 GFP exon trap, the RluA-2 GFP exon trap labelled nuclei. The nuclear localization for both RluA-1 and RluA-2 may indicate that these proteins act on RNA targets prior to export of the nucleus, or that they predominantly act upon nuclear localized RNAs. A caveat to this interpretation is that we have yet to demonstrate that these molecules function as genuine pseudouridine synthases, and this function remains a hypothesis that is based on the known function of evolutionary homologues. This hypothetical function requires future biochemical verification.

We also observed that *RluA-1* mutants showed an increase in the number of dendrite branches relative to control genotypes as well as an increase in isoneuronal crossovers. Transcription factors, cytoskeletal regulators, motor proteins, secretory pathways and cell adhesion molecules all function in concert to develop and maintain optimum dendrite morphology (55). RluA-1 may modify RNAs for those genes that regulate dendritic morphology, or changes in the dendrite morphology could be an indirect consequence of neuronal sensitivity that is regulated by RluA-1. It is noteworthy that prior studies have noted a potential link between the degree of dendrite branching and the sensitivity of nociception behaviors (20). In other cases, axonal factors such as the ion channel SK have been found to be important in regulating the cIVda neuron excitability (56, 57). Whether the dendrite branching phenotype that we observe in *RluA-1* mutants is a cause or a consequence of hypersensitivity will be an interesting question for future studies.

A large body of literature indicates that RNA trafficking and local translation is important in dendrites and axons of neurons (58, 59). Relative to uridine the pseudourine base

is believed to have enhanced rotational freedom which may alter conformation of RNA secondary structures. As well, an additional hydrogen bond donor present in pseudouridine may favor alternative base-pairing interactions in RNA. These properties may consequently alter RNA localization, stability and/or efficiency of translation (60-62). Pseudouridines can also influence decoding during translation as pseudouridylation of nonsense codons has been shown to suppress translation termination both *in vitro* and *in vivo* (63). Thus, another possible function for pseudouridylation in nociceptive neurons could be to favor read-through of pseudouridylated stop codons to generate novel sequences at protein carboxy termini.

The precise mechanism explaining the involvement of RluA proteins in nociception can only be elucidated by identifying the RNA targets of these enzymes. Several groups have developed methods using next generation sequencing methods to identify the pseudouridine sites in transcriptomes (30-33, 64). Future investigations applying these methods to wild type and *RluA* mutants in *Drosophila* will help us to identify the RluA targets and to further define the underlying mechanisms.

Materials and methods

Fly strains and husbandry

The following fly strains were obtained from Bloomington Stock Center: (w^{1118}; *PBac{vas-Cas9}VK00027*), *Mi{MIC}RluA-1*$^{[MI06897]}$, *Mi{MIC}RluA-2*$^{[MI12981]}$, *Df(2L)Exel7048/CyO*, (*yw; Sp/CyO; pC-(lox-attB2-SA-T2A-Gal4-Hsp70)3*), (*yw hs-cre, vasΦC31; Sp/CyO; Sb/TM3Ser*), (*P{ry=hsFLP}, yw M{vas-int.B}ZH-2A; Sp/CyO*; *P{FRT-attB-{GFSTF}-attB(w+)-FRT}*), *ppk-CD4-tdTom*, *md-Gal4*, *UAS-mCD8::RFP*, *40XUAS-mCD8::GFP*. The following fly strains were obtained from Exelixis collection at Harvard Medical School: *PBac{WH}*^{f02750}, *P{XP}d2586*, *PBac{WH}Grip75*$^{[f05483]}$, *PBac{WH}RluA-2*$^{[f07702]}$. The RNAi lines targeting *RluA-1* (31719-R1, 31719-R2) were obtained from Kyoto Stock Center. The genetic duplication line (BAC ID: CH321-

49P21) covering *RluA-1* (starting at 24,819,420 and ending at 24,910,132 on 2R) was obtained from Genetivision. The nos-Cas9 line used for generating *RluA-2*$^{del\text{-}HDR}$ and double mutant *RluA-1*$^{del\text{-}HDR}$*RluA-2*$^{del\text{-}HDR}$ [*y sc v; {nos-Cas9} attP2* (TH00787.N)] was kindly provided by the Norbert Perrimon lab. All larvae used in experiments were reared on the Bloomington *Drosophila* medium in an incubator with controlled temperature (25°C) and humidity (70%) on a 12h light/12h dark cycle. Strains were otherwise maintained at room temperature.

CRIPSR targeting of *RluA-1* and *RluA-2*

HDR for mutagenesis used the CRISPR/Cas9 (Gratz et al. 2013) to generate *RluA-1*$^{del\text{-}HDR}$, *RluA-2*$^{del\text{-}HDR}$ and the double mutant *RluA-1*$^{del\text{-}HDR}$*RluA-2*$^{del\text{-}HDR}$. Target sites were selected using the flyCRISPR Optimal Target Finder. For the precise deletion of *RluA-1*, the gRNA target sites are 5′ end 5′-CCACTG│TGCAGCGGAAAATTCAC-3′ (where "│" represents the Cas9 cut site, which is 71bp upstream of the *RluA-1* transcriptional start) and 3′ end: 5′-ACATATATTCAAAAGCT│CTTTGG-3′ (cut site at 60bp downstream of *RluA-1* 3′UTR). We used the following primer pairs to amplify the 885bp *RluA-1* homology ARM1: *RluA-1*-ARM1F: 5′-AATACACCTGCATTATCGCTGGTCCCTGTGGCTTTGCAC-3′,
RluA-1-ARM1R: 5′-AATACACCTGCAATTCTACCAGTGGGGCAAACCGCATTT-3′. We used *RluA-1*-ARM2F: 5′-GACTGCTCTTCGTATCTTTGGATGGTAAGTGCTTAAAC-3′ and *RluA-1*-ARM2R: 5′-ATTAGCTCTTCTGACCTTACAACTCCTTCAAGTCA-3′ to amplify 969 bp of *RluA-1* homology ARM2. For *RluA-2*, we used a target site at the 5′ end: 5′-GCAATCTATAGGTCTGC│GGAAGC-3′ (cut site at bp 5 of exon 3) and at the 3′ end: 5′AAGATAAACTACAGAGA│CCCCGG-3′ (cutting site in the middle of exon 8) so that the conserved pseudouridine synthase domain (located in exon 5) would be deleted. Primer pairs *RluA-2*-ARM1F: 5'CTAACACCTGCATATTCGCTCGAAACCCATTGTTAGCTG3′ and *RluA-2* ARM1R: 5′ CATTCACCTGCATTACTACGCAGACCTATAGATTGCAAT3′ were used to amplify the 979bp

348 *RluA-2* homology ARM1. *RluA-2*-ARM2F: 5'CAGTGCTCTTCGTATCCCCGGCACAAAGGATCTCA-
349 3', and *RluA-2*-ARM2R: 5' GACTGCTCTTCCGACATTTCAATGCCCTTGGCCAA-3' were used to
350 amplify the RluA-2 ARM2 (998bp). Rapid dsDNA donor cloning was carried out with the *pHD-*
351 *DsRed-attP* vector (65) and the guide RNA (gRNAs) were cloned into *pU6-BsbI-chiRNA* vector
352 (66). Embryos of *vas-Cas9* on chromosome III (w^{1118}; *PBac{y[+mDint2]=vas-Cas9}VK00027*,
353 "injection line 1") were injected with *RluA-1* dsDNA donor and gRNAs to generate G_0 founders
354 for $RluA\text{-}1^{del\text{-}HDR}$. Embryos with *nos-Cas9* on chromosome III [*y sc v; {nos-Cas9}attP2* (TH00787.N),
355 "injection line 2"] were injected with *RluA-2* dsDNA donor and gRNAs to create the G_0 founders
356 for $RluA\text{-}2^{del\text{-}HDR}$. For generating the double mutant $RluA\text{-}1^{del\text{-}HDR}RluA\text{-}2^{del\text{-}HDR}$, *nos-Cas9* was first
357 introduced to the $RluA\text{-}1^{del\text{-}HDR}$ mutant background and the DsRed marker in $RluA\text{-}1^{del\text{-}HDR}$
358 removed with CRE recombinase and the resultant homozygous strain [*yw*; $RluA\text{-}1^{del\text{-}HDR}\Delta DsRed$;
359 *{nos-Cas9}attP2* (TH00787.N), "injection line 3"] was injected with the *RluA-2* dsDNA donor and
360 gRNAs. All embryo injections of the dsDNA donor (at a concentration of 500ng/ul) and gRNAs
361 (100ng/ul for each) were performed by the Model system Injections
362 (modelsysteminjections@flymsi.com).

363 To identify the desired HDR mutants, G_0 flies were crossed to w^{1118} and single F_1
364 founders were identified with DsRed fluorescence in the eyes (from *3XP3-DsRed reporter*) and
365 mated with a second chromosome balancer strain to establish independent lines. Molecular
366 testing for the desired events was performed by PCR on gDNA extracted from candidates
367 placed over a deficiency (*Df(2L)Exelixis7048*) covering the *RluA-1* and *RluA-2* region (primer
368 pairs marked in **S2A** and **S4A Figs**). PCR products sequenced across the *attp-loxP-3XP3-DsRed-*
369 *SV40-loxP* fragment (**S2B** and **S4B Figs, Fig 4C**) confirmed accurate targeting of the loci. For
370 behavioral analysis, the original deletion mutants were backcrossed to *CS*, w^{1118} or isow^{1118} for
371 six times. For each generation, five heterozygous females were selected for six successive

backcrosses in vials and about 10 heterozygous females were used to cross to a second chromosome balancer to produce balanced mutant males in bottles and finally heterozygous mutant virgins and balanced males were crossed "en masse" in bottles to establish the balanced and homozygous mutant lines. In all crosses the dsRed fluorescence marker was used to follow the presence of the mutant.

Generation of deletion line in *RluA-1* and *RluA-2* using FRT-mediated deficiency

FRT bearing insertions *{WH+}*^{f02750} and *{XP-}*^{d2586} and in *RluA-1* (locations marked in **S2A Fig**) were used for generating a deficiency allele *RluA-1*$^{del\text{-}FRT}$. Insertions of *{WH-}RluA-2*^{F07702} and *{WH-}Grip75*^{f05483} (locations marked in **S4A Fig**) were used for generating the deficiency allele *RluA-2*$^{del\text{-}FRT}$. Crossing and heat-shock schemes followed (49). Hybrid PCR with corresponding primers (WH5′ plus / XP5′ minus left and right primers) was used to screen for candidate lines with *w-* deletion in *RluA-1*$^{del\text{-}FRT}$ and two-sided PCR with left and right primers for WH3′ minus/ WH5′ minus was used for screening for candidate lines with *w+* deletion in *RluA-2*$^{del\text{-}FRT}$ *(49).* Molecular testing for the deletion was performed by PCR on gDNA extracted from positive candidates placed over a deficiency (*Df(2L)Exelixis7048*) covering the *RluA-1* and *RluA-2* region. The primers used for PCR and sequencing verification in *RluA-1*$^{del\text{-}FRT}$ are *RluA-1-d2586*-up-F: 5′-AAAAATGCGGTTTGCCCC-3′, located upstream of the *{XP-}d2586* insertion site and *RluA-1-f02750*-down-R: 5′-AAGGGGTAACAAAAGTCCAG-3′, downstream of *{WH+}f02750 insertion site.*

Generation of *RluA-1*^{GAL4} using "Trojan-exon"

A triplet Trojan exon donor line on the 3rd chromosome *(yw; Sp/CyO; pC-(lox-attB2-SA-T2A-Gal4-Hsp70)3)* and an *RluA-1* insertion line containing an intronic MiMIC element (*Mi{MIC}RluA-1*$^{[MI06897]}$) were used to generate the *RluA-1*^{Gal4} driver using a crossing scheme as described by (45). Candidate males who have lost the y^+ selection marker associated with *MiMIC* were crossed to *40XUAS-mCD8::GFP* line and animals expressing GFP were selected to

396 establish a stable line. The line with the correct linker (phase 0) was confirmed with sequencing
397 of PCR products amplifying the left side with primers *RluA-1*-5494F: 5′-
398 TGATGTTGCCCCATAACG-3′ and *T2A-Gal4*-Seq-1R: 5' CGCTATCGATGCTCACGGTC-3′ and the
399 right side with the primers *T2A-Gal4*-4F: 5'-ACACCGTGCTGATGCTGC-3′ and *RluA-1*-5907R: 5′-
400 GAAAACATCGCACATCTGG-3′ of the *RluA-1* genome-*T2A-Gal4* insertion bordering region.

401 **Generation of GFSTF insertions in RluA-1 and RluA-2 by recombination mediated**
402 **cassette exchange (RMCE)**

403 Crossing, heat shocking and screening for EGFP tagged MiMIC lines in *RluA-1* and *RluA-2* were
404 essentially carried out as described (46). Males carrying a MiMIC insertion in a coding intron of
405 *RluA-1* (*RluA-1*^{MI06897}) or *RluA-2* (*RluA-2*^{MI12981}) were crossed to females carrying the *hs-FLP* and
406 *vasa-phiC31* integrase on the X chromosome and a frame-specific ("phase 0") *FRT* flanked
407 multiple tag (*GFSTF*) cassette on chromosome III. Candidate males with mosaic *w*- eyes and *y*-
408 bodies were individually crossed to *w; Sco/CyO; Sb/TM3 Ser* balancers to establish stocks. The
409 presence and direction of the insertion were tested by PCR assays described (67). Since the
410 original MiMIC insertion in *RluA-1* or *RluA-2* and the respective gene are in the same orientation,
411 positive PCR reaction 1 (with primers MiLF and TagR) and 4 (with primers MilR and TagF) as
412 described (67) indicated a successful RMCE event and resulted in expression.

413 **Generation of *UAS-RluA-1***

414 *Drosophila RluA-1* full length cDNA clone for *RluA-1* transcript A (FI04540) was obtained
415 from the Drosophila Genome Resource Center (DGRC). The *UAS-RluA-1* expression constructs
416 were generated with the ENTR/gateway system following the instructions of the manufacturer
417 (Invitrogen). The *RluA-1*-cDNA-F (5′-CACCATGCAGAATTCTCCGGCT-3′, and *RluA-1*-
418 cDNA+STOP-R (5′-TCATGCCGAGTCTAAGTG-3′ primers were used to amplify the open reading
419 frame and cloned into *pENTR-D-TOPO* vector. The sequence was verified and then cloned to

the P-element based destination vector *pTW*. Model System Injections performed injections into w^{1118} embryos. F_0 flies were crossed to w^{1118} and single F_1 founders were identified based on the w^+ marker. Individual lines were mapped and balanced to establish stable stocks. A *UAS-RluA-1* line with relatively weak expression evaluated by Q-PCR in *RluA-1*-cDNA lines driven by *md-GAL4* was used for the cIV-neuron specific *RluA-1*-cDNA rescue experiment (**Fig 3B**).

Larval behavioral analyses

Wandering 3rd instar larvae were washed out from vials and acclimated for 5 min in petri dishes before testing. Larval thermal and mechanical nociception response assays were conducted as previously described (4, 17, 56). Behavioral recording and scoring were performed with the observer blinded to the genotype.

For gentle touch assays, early L3 larvae were scooped out from the top layer of the fly food in the vials and 5-10 larvae were briefly rinsed with PBS and allowed to acclimate on 1% agarose in a plate for 5 min before testing with an eyelash fixed to the end of a paintbrush. Each larva was brushed with the eyelash on segments T1-A3 for 4 times and the responses were recorded and summarized using a gentle touch scale (68).

Immunohistochemistry and microscopy

The following primary antibodies were used for immunofluorescence: rabbit anti-GFP (ab6556, Abcam, 1:500), mouse anti-GFP (ab38689, Abcam, 1:500), Rabbit anti-HRP (1:100), mouse anti-nc82 (DSHB, supernatant, 1:30). Alexa Fluor 488, 633 were used at 1:1000 as secondary antibodies. Detailed immunostaining protocol is available on request. Images for immunostained tissues were taken on a Zeiss LSM 5 LIVE confocal microscope using a 40X objective except for **Fig 1D** and **S1B Fig**, which were taken on a Zeiss LSM880 using the 63X objective.

CIV dendrite imaging, tracing and analysis

To image class IV dendrites, the *DsRed* marker in *RluA-1*$^{del\text{-}HDR}$ was first removed with CRE recombinase (*w*^{1118}; *RluA-1*$^{del\text{-}HDR\Delta DsRed}$) and *ppk1.9-CD4::tdTom* was introduced to the mutant background and a stable homozygous stock was established. For CIV dendrite analysis, six virgins and three males were crossed in each vial for the mutant (*w*^{1118}; *RluA-1*$^{del\text{-}HDR\Delta DsRed}$; *ppk1.9-CD4::tdTom*) and control *(ppk1.9-CD4::-td-Tom*). Wandering larvae were anesthetized with diethyl ether in a sealed glass chamber for 15min before being arranged on a slide and covered with 50 mm glass coverslip. Neurons expressing the fluorescently tagged markers were visualized on a Zeiss LSM 5 Live confocal microscope with a 40X oil objective (Plan Apo M27, NA 0.8). Images were collected as 5x3 tiles scans of z-stacks with 512x512 resolution. A MatLab build was used for initial automatic tracing of the ddaC neuron dendrites from the confocal z-stack series TIFF images (69). The generated SWC files were overlaid onto the maximum intensity projected image of the neuron in neuTube (70) and manually curated to eliminate tracing errors made by MatLab. The corrected images were then analyzed with MatLab to extract neuron features of interest including number of branches, average branch length, and neuron size (the estimated size of the neuron, defined as the area of the minimum bounding circle) (69). Iso-neuronal crossover events were quantified manually from the traced dendrites for each genotype (n=6 neurons).

Statistical analysis

Statistics were performed using GraphPad Prism 4. Thermal and gentle touch behavioral data were compared with an unpaired non-parametric Mann-Whitney test when comparing two groups and Kruskal-Wallis test when comparing three or more groups. Mechanical nociception behavioral data were compared with Fisher's exact test. Dendrite morphology data were compared with the Student's t test. Error bars represent S.D. in all the figures unless otherwise specified.

Acknowledgements

The authors thank Drosophila Genomic Resource Center (supported by NIH grant 2P40OD010949) for clones. Stocks obtained from the Bloomington Drosophila Stock Center (NIH P40OD018537) were used in this study. We also thank the KYOTO Stock Center Kyoto in Kyoto Institute of Technology and Harvard Medical School for providing fly stocks used in this study. Members of Tracey lab provided helpful feedback on the manuscript and Jayce Brown Culbertson assisted with dendrite tracing.

References

1. Gaskin DJ, Richard P. The economic costs of pain in the United States. J Pain. 2012;13(8):715-24.

2. Tracey WD, Wilson RI, Laurent G, Benzer S. painless, a Drosophila gene essential for nociception. Cell. 2003;113(2):261-73.

3. Hwang RY, Zhong L, Xu Y, Johnson T, Zhang F, Deisseroth K, et al. Nociceptive neurons protect Drosophila larvae from parasitoid wasps. Curr Biol. 2007;17(24):2105-16.

4. Caldwell JC, Tracey WD. Alternatives to Mammalian Pain Models 2: Using Drosophila to Identify Novel Genes Involved in Nociception. Methods Mol Biol. 2010;617:19-29.

5. Milinkeviciute G, Gentile C, Neely GG. Drosophila as a tool for studying the conserved genetics of pain. Clin Genet. 2012;82(4):359-66.

6. Im SH, Galko MJ. Pokes, sunburn, and hot sauce: Drosophila as an emerging model for the biology of nociception. Dev Dynam. 2012;241(1):16-26.

7. Tracey WD, Jr. Nociception. Curr Biol. 2017;27(4):R129-R33.

8. Khuong TM, Wang QP, Manion J, Oyston LJ, Lau MT, Towler H, et al. Nerve injury drives a heightened state of vigilance and neuropathic sensitization in Drosophila. Sci Adv. 2019;5(7):eaaw4099.

9. Xiang Y, Yuan Q, Vogt N, Looger LL, Jan LY, Jan YN. Light-avoidance-mediating photoreceptors tile the Drosophila larval body wall. Nature. 2010;468(7326):921-6.

10. Grueber WB, Jan LY, Jan YN. Tiling of the Drosophila epidermis by multidendritic sensory neurons. Development. 2002;129(12):2867-78.

11. Hu C, Petersen M, Hoyer N, Spitzweck B, Tenedini F, Wang D, et al. Sensory integration and neuromodulatory feedback facilitate Drosophila mechanonociceptive behavior. Nat Neurosci. 2017;20(8):1085-95.

12. Ohyama T, Schneider-Mizell CM, Fetter RD, Aleman JV, Franconville R, Rivera-Alba M, et al. A multilevel multimodal circuit enhances action selection in Drosophila. Nature. 2015;520(7549):633-9.

13. Chin MR, Tracey WD, Jr. Nociceptive Circuits: Can't Escape Detection. Curr Biol. 2017;27(16):R796-R8.

14. Burgos A, Honjo K, Ohyama T, Qian CS, Shin GJ, Gohl DM, et al. Nociceptive interneurons control modular motor pathways to promote escape behavior in Drosophila. Elife. 2018;7.

15. Ohyama T, Jovanic T, Denisov G, Dang TC, Hoffmann D, Kerr RA, et al. High-throughput analysis of stimulus-evoked behaviors in Drosophila larva reveals multiple modality-specific escape strategies. Plos One. 2013;8(8):e71706.

16. Zhong L, Hwang RY, Tracey WD. Pickpocket is a DEG/ENaC protein required for mechanical nociception in Drosophila larvae. Curr Biol. 2010;20(5):429-34.

17. Mauthner SE, Hwang RY, Lewis AH, Xiao Q, Tsubouchi A, Wang Y, et al. Balboa Binds to Pickpocket In Vivo and Is Required for Mechanical Nociception in Drosophila Larvae. Curr Biol. 2014;24(24).

18. Gorczyca DA, Younger S, Meltzer S, Kim SE, Cheng L, Song W, et al. Identification of Ppk26, a DEG/ENaC Channel Functioning with Ppk1 in a Mutually Dependent Manner to Guide Locomotion Behavior in Drosophila. Cell Rep. 2014;9(4):1446-58.

19. Zhong L, Bellemer A, Yan H, Ken H, Jessica R, Hwang RY, et al. Thermosensory and nonthermosensory isoforms of Drosophila melanogaster TRPA1 reveal heat-sensor domains of a thermoTRP Channel. Cell Rep. 2012;1(1):43-55.

20. Honjo K, Mauthner SE, Wang Y, Skene JH, Tracey WD, Jr. Nociceptor-Enriched Genes Required for Normal Thermal Nociception. Cell Rep. 2016;16(2):295-303.

21. Brewster R, Bodmer R. Origin and specification of type II sensory neurons in Drosophila. Development. 1995;121(9):2923-36.

22. Wang CC, Lo JC, Chien CT, Huang ML. Spatially controlled expression of the Drosophila pseudouridine synthase RluA-1. Int J Dev Biol. 2011;55(2):223-7.

23. Olesnicky EC, Killian DJ, Garcia E, Morton MC, Rathjen AR, Sola IE, et al. Extensive use of RNA-binding proteins in Drosophila sensory neuron dendrite morphogenesis. G3 (Bethesda). 2014;4(2):297-306.

24. Ye B, Petritsch C, Clark IE, Gavis ER, Jan LY, Jan YN. Nanos and Pumilio are essential for dendrite morphogenesis in Drosophila peripheral neurons. Curr Biol. 2004;14(4):314-21.

25. Pan L, Zhang YQ, Woodruff E, Broadie K. The Drosophila fragile X gene negatively regulates neuronal elaboration and synaptic differentiation. Curr Biol. 2004;14(20):1863-70.

26. Brechbiel JL, Gavis ER. Spatial regulation of nanos is required for its function in dendrite morphogenesis. Curr Biol. 2008;18(10):745-50.

27. Bianco A, Dienstbier M, Salter HK, Gatto G, Bullock SL. Bicaudal-D regulates fragile X mental retardation protein levels, motility, and function during neuronal morphogenesis. Curr Biol. 2010;20(16):1487-92.

28. Xu X, Brechbiel JL, Gavis ER. Dynein-dependent transport of nanos RNA in Drosophila sensory neurons requires Rumpelstiltskin and the germ plasm organizer Oskar. J Neurosci. 2013;33(37):14791-800.

29. Ge J, Yu YT. RNA pseudouridylation: new insights into an old modification. Trends Biochem Sci. 2013;38(4):210-8.

30. Carlile TM, Rojas-Duran MF, Zinshteyn B, Shin H, Bartoli KM, Gilbert WV. Pseudouridine profiling reveals regulated mRNA pseudouridylation in yeast and human cells. Nature. 2014;515(7525):143-+.

31. Lovejoy AF, Riordan DP, Brown PO. Transcriptome-Wide Mapping of Pseudouridines: Pseudouridine Synthases Modify Specific mRNAs in S. cerevisiae. Plos One. 2014;9(10).

32. Schwartz S, Bernstein DA, Mumbach MR, Jovanovic M, Herbst RH, Leon-Ricardo BX, et al. Transcriptome-wide mapping reveals widespread dynamic-regulated pseudouridylation of ncRNA and mRNA. Cell. 2014;159(1):148-62.

33. Khoddami V, Yerra A, Mosbruger TL, Fleming AM, Burrows CJ, Cairns BR. Transcriptome-wide profiling of multiple RNA modifications simultaneously at single-base resolution. Proc Natl Acad Sci U S A. 2019;116(14):6784-9.

34. Knight SW, Heiss NS, Vulliamy TJ, Greschner S, Stavrides G, Pai GS, et al. X-linked dyskeratosis congenita is predominantly caused by missense mutations in the DKC1 gene. Am J Hum Genet. 1999;65(1):50-8.

35. Fujiwara T, Harigae H. Pathophysiology and genetic mutations in congenital sideroblastic anemia. Pediatr Int. 2013;55(6):675-9.

36. de Brouwer APM, Abou Jamra R, Kortel N, Soyris C, Polla DL, Safra M, et al. Variants in PUS7 Cause Intellectual Disability with Speech Delay, Microcephaly, Short Stature, and Aggressive Behavior. Am J Hum Genet. 2018;103(6):1045-52.

563 37. Hammal T, Ferre-D'Amare AR. Pseudouridine synthases. Chem Biol. 2006;13(11):1125-
564 35.
565 38. Koonin EV. Pseudouridine synthases: four families of enzymes containing a putative
566 uridine-binding motif also conserved in dUTPases and dCTP deaminases. Nucleic Acids Res.
567 1996;24(12):2411-5.
568 39. Phillips B, Billin AN, Cadwell C, Buchholz R, Erickson C, Merriam JR, et al. The Nop60B
569 gene of Drosophila encodes an essential nucleolar protein that functions in yeast. Mol Gen
570 Genet. 1998;260(1):20-9.
571 40. Giordano E, Peluso I, Senger S, Furia M. minifly, a Drosophila gene required for
572 ribosome biogenesis. J Cell Biol. 1999;144(6):1123-33.
573 41. Vicidomini R, Petrizzo A, di Giovanni A, Cassese L, Lombardi AA, Pragliola C, et al.
574 Drosophila dyskerin is required for somatic stem cell homeostasis. Sci Rep. 2017;7(1):347.
575 42. Hoang C, Chen JJ, Vizthum CA, Kandel JM, Hamilton CS, Mueller EG, et al. Crystal
576 structure of pseudouridine synthase RluA: Indirect sequence readout through protein-induced
577 RNA structure. Mol Cell. 2006;24(4):535-45.
578 43. Gutgsell NS, Deutscher MP, Ofengand J. The pseudouridine synthase RluD is required
579 for normal ribosome assembly and function in Escherichia coli. Rna. 2005;11(7):1141-52.
580 44. Raychaudhuri S, Niu L, Conrad J, Lane BG, Ofengand J. Functional effect of deletion
581 and mutation of the Escherichia coli ribosomal RNA and tRNA pseudouridine synthase RluA. J
582 Biol Chem. 1999;274(27):18880-6.
583 45. Diao F, Ironfield H, Luan H, Diao F, Shropshire WC, Ewer J, et al. Plug-and-play genetic
584 access to drosophila cell types using exchangeable exon cassettes. Cell Rep. 2015;10(8):1410-21.
585 46. Nagarkar-Jaiswal S, DeLuca SZ, Lee P-T, Lin W-W, Pan H, Zuo Z, et al. A genetic toolkit
586 for tagging intronic MiMIC containing genes. Elife. 2015;4.

47. Ainsley JA, Pettus JM, Bosenko D, Gerstein CE, Zinkevich N, Anderson MG, et al. Enhanced locomotion caused by loss of the Drosophila DEG/ENaC protein Pickpocket1. Curr Biol. 2003;13(17):1557-63.

48. Ran FA, Hsu PD, Wright J, Agarwala V, Scott DA, Zhang F. Genome engineering using the CRISPR-Cas9 system. Nat Protoc. 2013;8(11):2281-308.

49. Parks AL, Cook KR, Belvin M, Dompe NA, Fawcett R, Huppert K, et al. Systematic generation of high-resolution deletion coverage of the Drosophila melanogaster genome. Nat Genet. 2004;36(3):288-92.

50. Venken KJ, Carlson JW, Schulze KL, Pan H, He Y, Spokony R, et al. Versatile P[acman] BAC libraries for transgenesis studies in Drosophila melanogaster. Nat Methods. 2009;6(6):431-4.

51. Han C, Wang D, Soba P, Zhu S, Lin X, Jan LY, et al. Integrins regulate repulsion-mediated dendritic patterning of drosophila sensory neurons by restricting dendrites in a 2D space. Neuron. 2012;73(1):64-78.

52. Kim SE, Coste B, Chadha A, Cook B, Patapoutian A. The role of Drosophila Piezo in mechanical nociception. Nature. 2012;483(7388):209-12.

53. Tenenbaum CM, Misra M, Alizzi RA, Gavis ER. Enclosure of Dendrites by Epidermal Cells Restricts Branching and Permits Coordinated Development of Spatially Overlapping Sensory Neurons. Cell Rep. 2017;20(13):3043-56.

54. Meltzer S, Yadav S, Lee J, Soba P, Younger SH, Jin P, et al. Epidermis-Derived Semaphorin Promotes Dendrite Self-Avoidance by Regulating Dendrite-Substrate Adhesion in Drosophila Sensory Neurons. Neuron. 2016;89(4):741-55.

55. Corty MM, Matthews BJ, Grueber WB. Molecules and mechanisms of dendrite development in Drosophila. Development. 2009;136(7):1049-61.

611 56. Walcott KCE, Mauthner SE, Tsubouchi A, Robertson J, Tracey WD. The Drosophila
612 Small Conductance Calcium-Activated Potassium Channel Negatively Regulates Nociception.
613 Cell Rep. 2018;24(12):3125-32 e3.
614 57. Onodera K, Baba S, Murakami A, Uemura T, Usui T. Small conductance Ca(2+)-
615 activated K(+) channels induce the firing pause periods during the activation of Drosophila
616 nociceptive neurons. Elife. 2017;6.
617 58. Rangaraju V, Tom Dieck S, Schuman EM. Local translation in neuronal compartments:
618 how local is local? EMBO Rep. 2017;18(5):693-711.
619 59. Glock C, Heumuller M, Schuman EM. mRNA transport & local translation in neurons.
620 Curr Opin Neurobiol. 2017;45:169-77.
621 60. Arnez JG, Steitz TA. Crystal structure of unmodified tRNA(Gln) complexed with
622 glutaminyl-tRNA synthetase and ATP suggests a possible role for pseudo-uridines in
623 stabilization of RNA structure. Biochemistry-Us. 1994;33(24):7560-7.
624 61. Newby MI, Greenbaum NL. Sculpting of the spliceosomal branch site recognition motif
625 by a conserved pseudouridine. Nat Struct Biol. 2002;9(12):958-65.
626 62. Kariko K, Muramatsu H, Welsh FA, Ludwig J, Kato H, Akira S, et al. Incorporation of
627 pseudouridine into mRNA yields superior nonimmunogenic vector with increased translational
628 capacity and biological stability. Mol Ther. 2008;16(11):1833-40.
629 63. Karijolich J, Yu YT. Converting nonsense codons into sense codons by targeted
630 pseudouridylation. Nature. 2011;474(7351):395-+.
631 64. Li XY, Zhu P, Ma SQ, Song JH, Bai JY, Sun FF, et al. Chemical pulldown reveals dynamic
632 pseudouridylation of the mammalian transcriptome. Nat Chem Biol. 2015;11(8):592-U93.
633 65. Beumer KJ, Carroll D. Targeted genome engineering techniques in Drosophila.
634 Methods. 2014;68(1):29-37.

635 66. Gratz SJ, Cummings AM, Nguyen JN, Hamm DC, Donohue LK, Harrison MM, et al.
636 Genome engineering of Drosophila with the CRISPR RNA-guided Cas9 nuclease. Genetics.
637 2013;194(4):1029-35.
638 67. Venken KJT, Schulze KL, Haelterman NA, Pan H, He Y, Evans-Holm M, et al. MiMIC: a
639 highly versatile transposon insertion resource for engineering Drosophila melanogaster genes.
640 Nat Methods. 2011;8(9):737-43.
641 68. Tsubouchi A, Caldwell JC, Tracey WD. Dendritic filopodia, Ripped Pocket, NOMPC, and
642 NMDARs contribute to the sense of touch in Drosophila larvae. Curr Biol. 2012;22(22):2124-34.
643 69. Gulyanon S, Sharifai, N., Kim, M. D., Chiba, A., Tsechpenakis, G. CRF formulation of
644 active contour population for efficient three-dimensional neurite tracing. 2016 IEEE 13th
645 International Symposium on Biomedical Imaging2016. p. 593-7.
646 70. Feng L, Zhao T, Kim J. neuTube 1.0: A New Design for Efficient Neuron Reconstruction
647 Software Based on the SWC Format. eNeuro. 2015;2(1).
648

649 ## Figure Legends

650 **Fig 1**. ***RluA-1* gene and protein expression in *Drosophila melanogaster*.** (**A**) A low
651 magnification confocal micrograph of *RluA-1* gene expression pattern in the larval PNS (third
652 instar w^{1118}; *RluA-1*^{Gal4}/*4oxUAS-mCD8::GFP*). Note that GFP positive signals are detected in
653 peripheral sensory neurons in each segment along the larval body wall. Scale bar=500μm. (**B**)
654 Higher magnification of an abdominal dorsal PNS cluster. *RluA-1*^{Gal4} is expressed in the cell body
655 and dendrites of all classes of multidendritic neurons, external sensory (ES), dorsal multiple
656 dendrite neuron (dmd1) and dorsal bipolar dendritic (dbd) neurons (ddaD and ddaE (Class I),
657 ddaB (Class II), ddaA and ddaF (Class III), and ddaC (ClassIV), ES, dmd1 and dbd neurons are
658 labeled). Scale bar = 50μm. (**C**). *RluA-1*^{Gal4}/+ driving expression of *4oxUAS-mCD8::GFP*/+ in the

659 larval CNS. Labelling is observed in axonal projections of sensory neurons in the larval ventral
660 nerve cord and unidentified clusters of neurons in the larval brain. Scale bar =5 0μm. (**D^{1-3}**) anti-
661 GFP immunohistochemistry of a third instar larval fillet preparation of *RluA-1-GFSTF/*
662 *Gal4109(2)80>UAS-mCD8-RFP*, immunoreactive signals are detected in the nuclei of multi-
663 dendritic neurons (D^1 green, GFP) surrounded by the membrane-localized RFP signal (D^2
664 magenta, RFP) and merged image in D^3. Scale bar = 50μm.

665 **Fig 2. Thermal nociception in animals with *RluA-1* loss of function. (A).** Class IV specific
666 knock-down in *RluA-1* results in significant hypersensitive thermal nociception in larvae
667 compared to the *ppk-GAL4* driver alone animals at 46 (average latency of 1.33 ± 1.10 sec for
668 *ppk-Gal4 > UAS-RluA-1-RNAi (*31719-R1*)*, n=38 vs. 2.04 ± 1.89 sec for *ppk-GAL4* driver alone,
669 n=37. P<0.05), albeit not statistically significant compared to the UAS-RNAi alone (1.96 ± 1.32
670 sec for UAS-RNAi alone, n=27). These differences are more pronounced at 42 (average latency
671 of 1.92 ± 1.16 sec for *ppk-Gal4 > UAS-RluA-1-RNAi*, n=35 vs. 6.25 ± 2.51 sec for *ppk-GAL4* driver
672 alone controls, n=42 or 5.20 ± 3.28 sec for UAS-RNAi alone controls, n=49, P<0.0001). Kruskal-
673 Wallis test with Dunn's multiple comparison tests, only significant comparisons were labeled.
674 **(B).** Homozygous null mutant *RluA-1$^{del\text{-}HDR}$* larvae showed significantly faster response to
675 noxious heat stimulation of 42°C compared to the corresponding control animals of *Canton-S*
676 (average latency of 1.29 ± 0.78 sec in *RluA-1$^{-/-}$*, n=54 vs. 2.22 ± 1.32 sec in *CS*, n=39), *w^{1118}* (2.23 ±
677 1.57 sec in *RluA-1$^{-/-}$*, n=51 vs. 4.16 ± 2.31 sec in *w^{1118}*, n=36) and iso*w^{1118}* (4.82 ± 2.53 sec in *RluA-1$^{-/-}$*,
678 n=30 vs. 11.99 ± 3.98 sec in iso*w^{1118}*, n=17). Significance of comparisons are marked as ****
679 (p<0.0001). Data were analyzed using Mann-Whitney non-parametric test. **(C).**
680 Transheterozygote *RluA-1$^{del\text{-}HDR}$/RluA-1$^{del\text{-}FRT}$* showed hypersensitive thermal nociception
681 responses compared to the controls (average latency of 3.07 ± 1.72 sec in *RluA-1$^{del\text{-}HDR}$/RluA-1$^{del\text{-}$*
682 *^{FRT}*, n=195 vs. 6.17 ± 3.95 sec in +/+, n=125). The genetic background is *w^{1118}* for *RluA-1$^{del\text{-}HDR}$*, and

683 isow^{1118} for *RluA-1*$^{del\text{-}FRT}$. For the *RluA-1*$^{del\text{-}HDR}$/*RluA-1*$^{del\text{-}FRT}$ transheterozygotes, data were pooled
684 from the progeny from reciprocal crosses of *RluA-1*$^{del\text{-}HDR}$ to *RluA-1*$^{del\text{-}FRT}$. To generate the control
685 larvae, reciprocal crosses were made between the genetic background of w^{1118} and isow^{1118} and
686 the data from the progeny of these crosses were pooled. Significance of the comparison is
687 marked as **** (exact p<0.0001). Data were analyzed using Mann-Whitney U test.

688 **Fig 3**: ***RluA-1* nociception phenotypes with (A) chromosome duplication or (B) Class IV-**
689 **specific expression of *UAS-RluA-1 cDNA*.** (**A**). The hypersensitive nociception phenotype with
690 42□ thermal stimulus in *RluA-1*$^{del\text{-}HDR}$ null mutant was rescued by introducing a duplication (Dp)
691 on the third chromosome which covers the *RluA-1* gene region (average latency of 8.02 ± 3.61
692 sec in *RluA-1*$^{-/-}$; Dp/Dp, n=38, which is similar to the isow^{1118} genetic background (+/+, average
693 latency of 10.16±3.87 sec, n=22) , but significantly slower than the latency of 5.31 ± 2.16 sec in
694 *RluA-1*$^{-/-}$, n=34 (p=0.02)). Larvae with one copy of duplication showed slower response (average
695 latency of 6.90 ± 4.81 sec in *RluA-1*$^{-/-}$; *Dp*/+, n=45) without statistical significance compared to
696 *RluA-1*$^{del\text{-}HDR}$. Data were analyzed using Kruskal-Wallis test with Dunn's multiple comparison
697 tests. (**B**). The hypersensitive thermal nociception phenotype in *RluA-1*$^{del\text{-}HDR}$ larvae was
698 completely reversed to that of the heterozygous *RluA-1* by Class IV specific expression of full
699 length *RluA-1-cDNA* (*RluA-1*$^{-/-}$; *ppk-Gal4*$^{+/-}$; *UAS-RluA-1*$^{+/-}$, average latency of 12.37 ±6.48 sec,
700 n=30, is similar to *RluA-1*$^{+/-}$; *ppk1.9-Gal4*$^{+/-}$, average latency of 11.04 ± 5.44 sec, n=20 but
701 significantly slower than either the driver alone (*RluA-1*$^{-/-}$; *Ppk1.9-Gal4*$^{+/-}$, average latency of
702 3.78±2.11 sec, n=25 or transgene alone controls (*RluA-1*$^{-/-}$; *UAS-RluA-1*$^{+/-}$, average latency of 2.86
703 ± 1.39 sec, n=33) at 42□ thermal stimulus. Significance of the comparisons are marked as ****
704 (p<0.0001). Data were analyzed using Kruskal-Wallis test with Dunn's multiple comparison tests.

705 **Fig 4**: ***RluA-1* mechanical nociception and gentle touch responses.** (**A**). In response to the
706 noxious mechanical stimulus of 30mN/720kPa, all (100%) of the *RluA-1*$^{del\text{-}HDR}$ null mutant larvae

(*RluA-1*$^{-/-}$, n=28) rolled compared to the 78.57% of control larvae (iso*w*^{1118} n=28) rolling. At the reduced stimulus of 15mN/360kPa, 95.56% of *RluA-1*$^{-/-}$ (n=45) rolled while only 48.53% of control (n=68) rolled. Significance of the comparisons are marked as *(p<0.05) and **** (p<0.0001). Data were analyzed using Fisher's exact test and presented as percentages ± 95% confidence intervals. (**B**). *RluA-1*$^{del\text{-}HDR}$ larvae (*RluA-1*$^{-/-}$) had a gentle touch response score (6.70 ± 2.48, n=36) similar to the control larvae (iso*w*^{1118}, 7.83 ± 2.69, n=30). ns, not significant (p>0.05). Data were analyzed with Student's t test.

Fig 5: **RluA-2 expression in *Drosophila* larvae.** (**A**). In third instar larvae of *RluA-2-GFSTF* line, anti-GFP (green) immunoreactive signals are detected in the nuclei of all types of cells (neurons are labelled with anti-HRP (red)). Scale bar = 100µm. (**B**). In the larval abdominal dorsal PNS cluster of *RluA-2-GFSTF* line, GFP signal (green) is also detected in the nuclei of the md neurons, whose membranes are marked with anti-HRP (magenta). Arrow points to Class IV ddaC neuron. Scale bar = 50µm.

Fig 6. **Thermal nociception responses of *RluA-1* and *RluA-2* single mutant, and *RluA-1 RluA-2* double mutant**. Larvae of single mutant *RluA-1*$^{del\text{-}HDR}$ (*RluA-1*$^{-/-}$), *RluA-2*$^{del\text{-}HDR}$ (*RluA-2*$^{-/-}$), double mutant *RluA-1*$^{del\text{-}HDR}$ *RluA-2*$^{del\text{-}HDR}$ (*RluA-1*$^{-/-}$ *RluA-2*$^{-/-}$) and the genetic background iso*w*^{1118} (+/+) were stimulated with noxious heat probe of 42□. *RluA-1*$^{-/-}$, *RluA-2*$^{-/-}$, and *RluA-1*$^{-/-}$ *RluA-2*$^{-/-}$ all displayed faster responses to the stimulus compared to controls (*RluA-1*$^{-/-}$ average latency of 4.32 ± 2.80 sec, n= 79; *RluA-2*$^{-/-}$, 6.63 ± 3.31 sec, n=68; (*RluA-1*$^{-/-}$*RluA-2*$^{-/-}$), 6.26 ± 3.46 sec, n=57; +/+, 13.72 ± 6.03 sec, n=46). Significance of comparisons are marked as ** (p<0.01), *** (p<0.001) or **** (p<0.0001). Data were analyzed using Kruskal-Wallis test with Dunn's multiple comparison tests.

Fig 7. ***RluA-1* ddaC neuron dendrite morphology.** (**A-C**). Quantification of the branch number (**A**), average branch length (**B**), and isoneuronal cross-over points (**C**). (**A**). Homozygous *RluA-*

731 $1^{del\text{-}HDR}$ larvae showed a higher normalized branch number (total number of branches / (neuron
732 size x $10^{-4}\mu m^2$), 32.56 ± 7.83 in *RluA-1*$^{-/-}$; *ppk-tdTom*, n=6 vs 23.10 ± 4.96 in *ppk-tdTom* control,
733 n=6, p<0.05). (**B**). The mean ddaC dendritic branch length in homozygous *RluA-1*$^{del\text{-}HDR}$ was
734 shorter than that of the control (average branch length is 14.01 ± 1.29 μm in *RluA-1*$^{-/-}$; *ppk-*
735 *tdTom*, n=6 vs 16.30 ± 1.07 μm in *ppk-tdTom* control, n=6, p<0.01). (**C**). The number of ddaC
736 dendritic isoneuronal crossovers in homozygous *RluA-1*$^{del\text{-}HDR}$ was higher compared to that of
737 the control (normalized crossover points = crossover points / (neuron size x $10^{-7}\mu m^2$), 25.03 ±
738 8.24 in *RluA-1*$^{-/-}$; *ppk-tdTom*, n=6 vs 13.48 ± 4.08 in *ppk-tdTom* control, n=6, p<0.05). Significant
739 differences are marked as * (p<0.05) and ** (p<0.01). Data were analyzed with Student's t test.
740 (**D**). Representative traced dendritic structure of a class IV ddaC neuron of an L3 larva
741 expressing *ppk-GAL4 > UAS-td-Tom* in homozygous *RluA-1*$^{del\text{-}HDR}$ (*RluA-1*$^{-/-}$, **left**) in comparison
742 with that of the *ppk-tdTom* control (+/+, **right**). The position of the cell body is marked with blue
743 circle and axon with red circles.

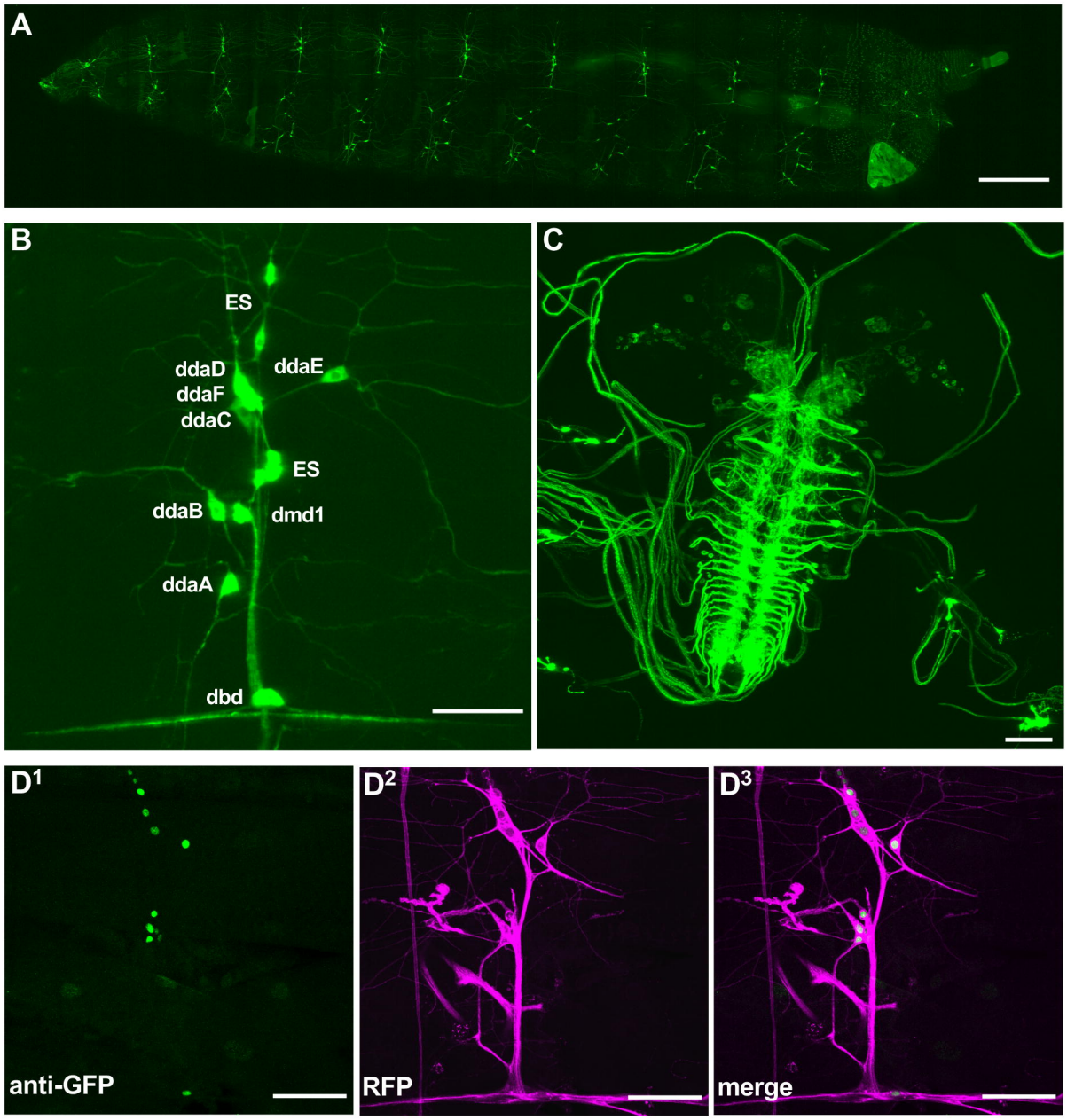
A
B
ES
ddaD
ddaE
ddaF
ddaC
ES
ddaB
dmd1
ddaA
dbd
C
D1
anti-GFP
D2
RFP
D3
merge

Figure 1

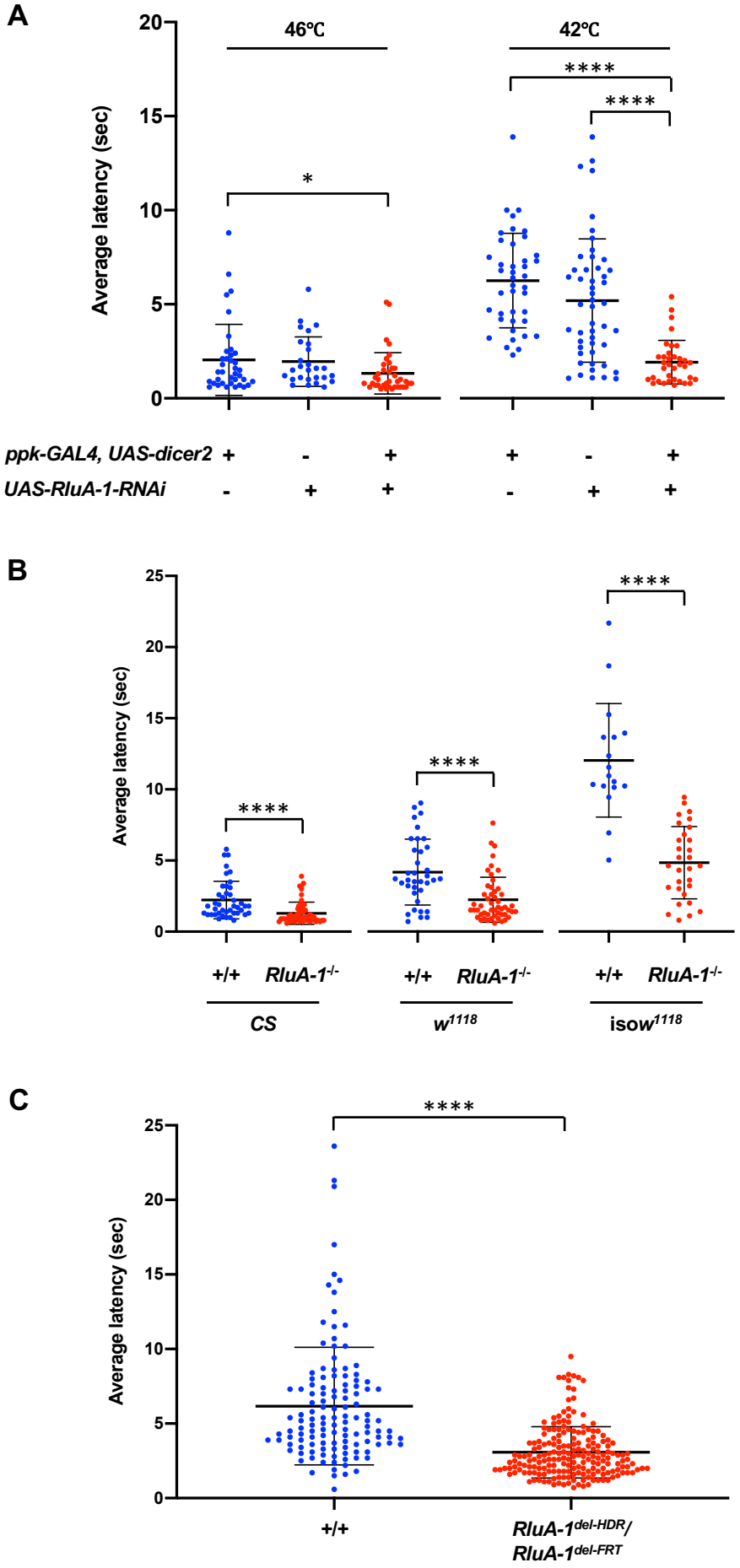
A
46°C
42°C
Average latency (sec)
20
15
10
5
0
*
****
****
ppk-GAL4, UAS-dicer2 + - + + - +
UAS-RluA-1-RNAi - + + - + +
B
Average latency (sec)
25
20
15
10
5
0
****
****
****
+/+ RluA-1-/-
CS
+/+ RluA-1-/-
w1118
+/+ RluA-1-/-
isow1118
C
Average latency (sec)
25
20
15
10
5
0
****
+/+
RluA-1del-HDR/
RluA-1del-FRT

Figure 2

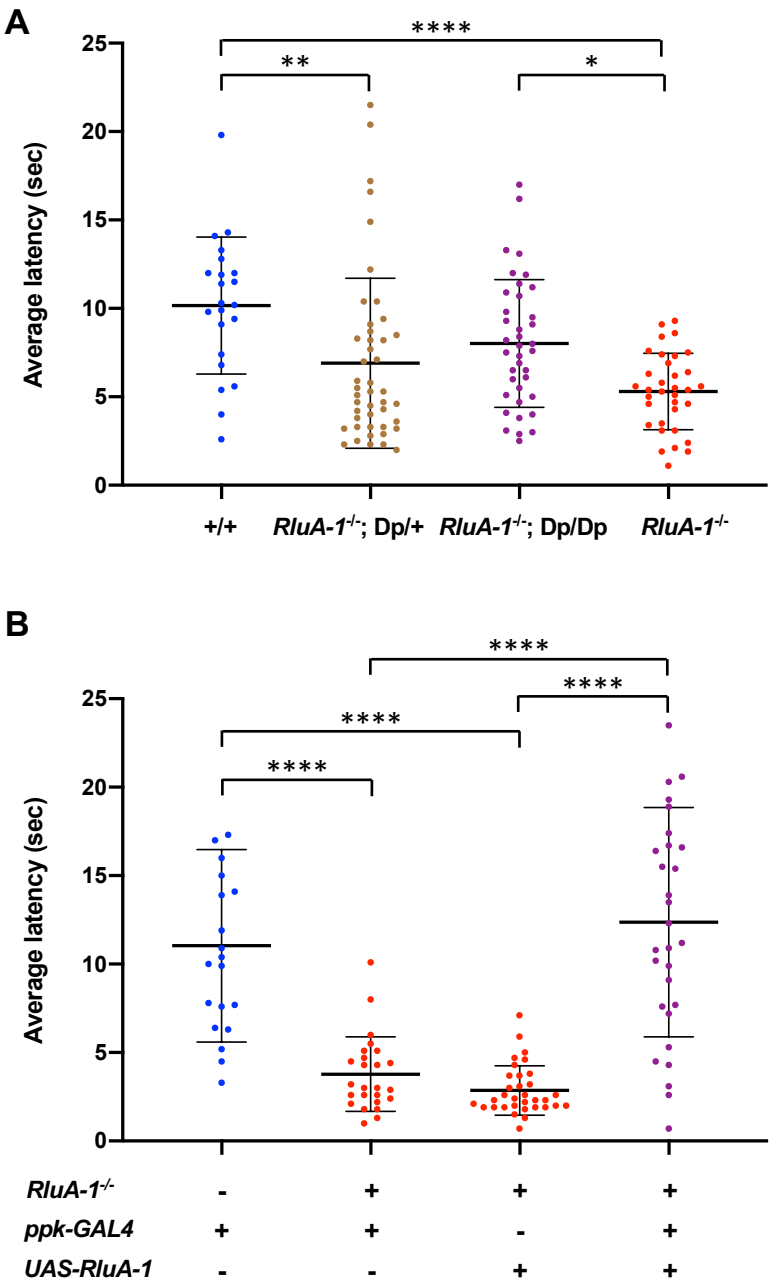
A
Average latency (sec)
25
20
15
10
5
0
****
**
*
+/+
RluA-1-/-; Dp/+
RluA-1-/-; Dp/Dp
RluA-1-/-
B
Average latency (sec)
25
20
15
10
5
0
****
****
****
****
RluA-1-/- - + + +
ppk-GAL4 + + - +
UAS-RluA-1 - - + +

Figure 3

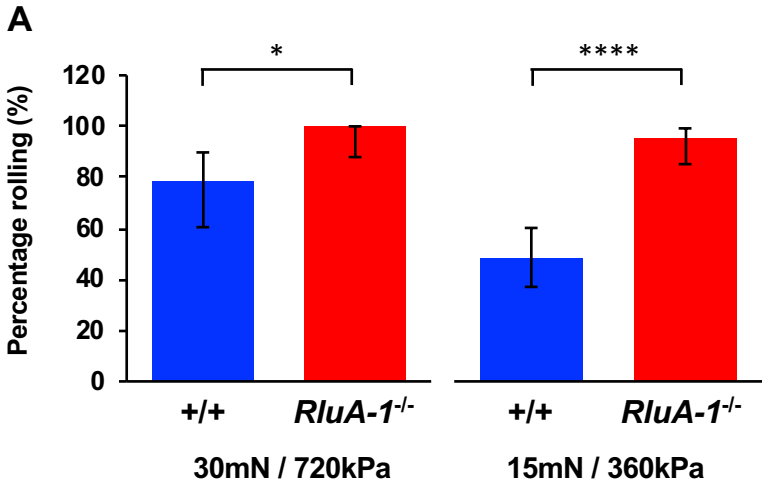
A
*
****
120
100
80
60
40
20
0
Percentage rolling (%)
+/+
RluA-1-/-
+/+
RluA-1-/-
30mN / 720kPa
15mN / 360kPa

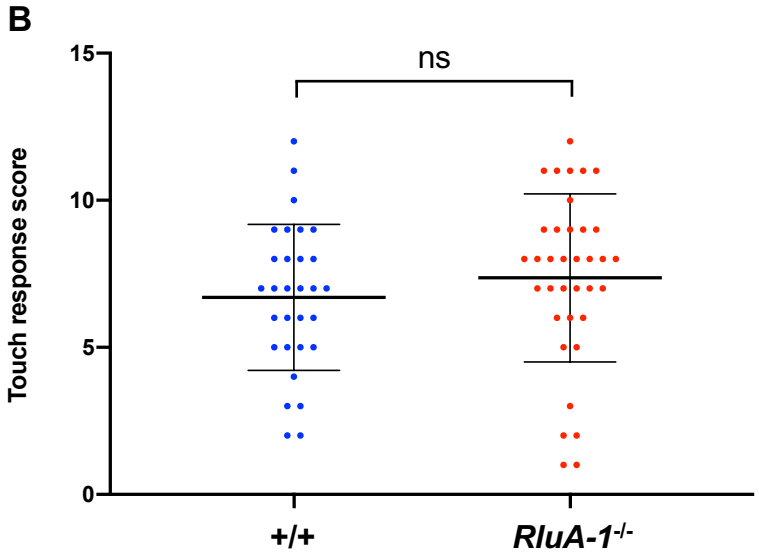
B
ns
15
10
5
0
Touch response score
+/+
RluA-1-/-

Figure 4

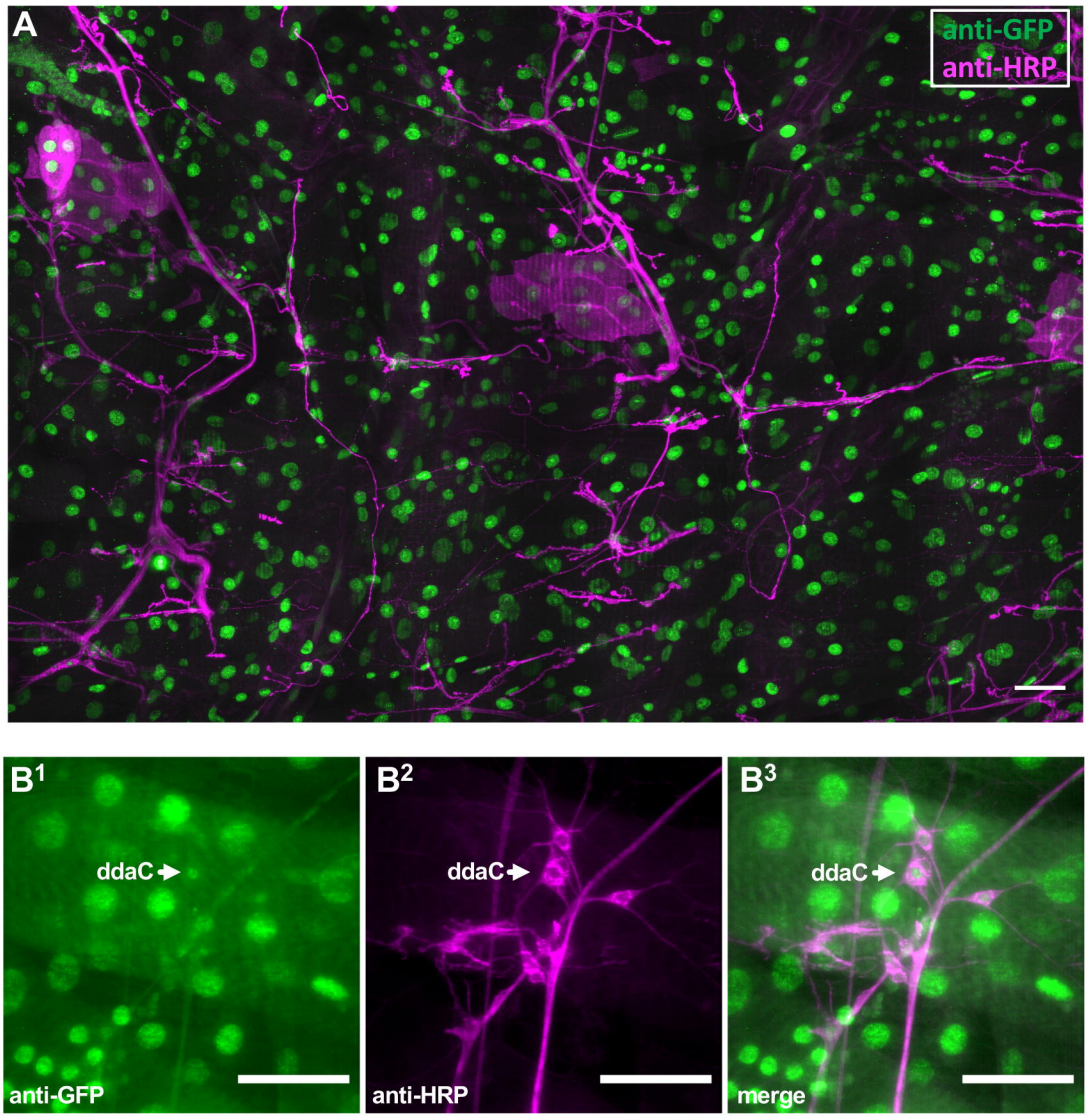
A
anti-GFP
anti-HRP
B1
ddaC
anti-GFP
B2
ddaC
anti-HRP
B3
ddaC
merge

Figure 5

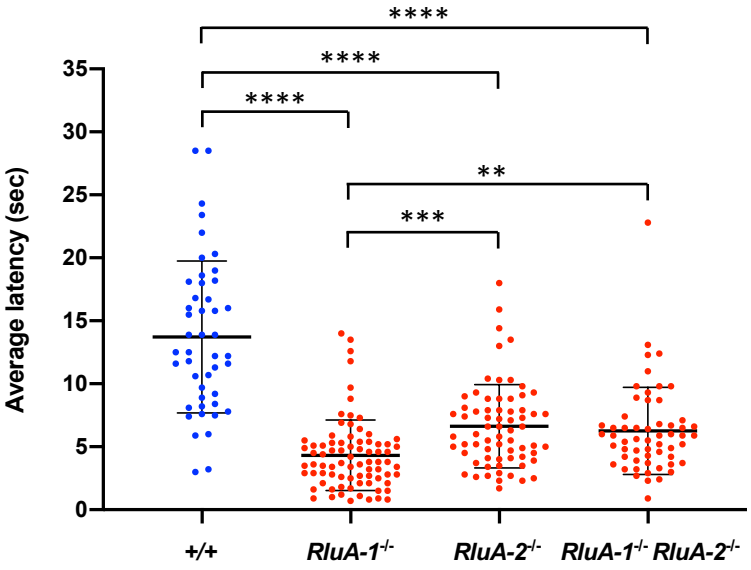
****
****
****
**
***
Average latency (sec)
35
30
25
20
15
10
5
0
+/+
RluA-1-/-
RluA-2-/-
RluA-1-/- RluA-2-/-

Figure 6

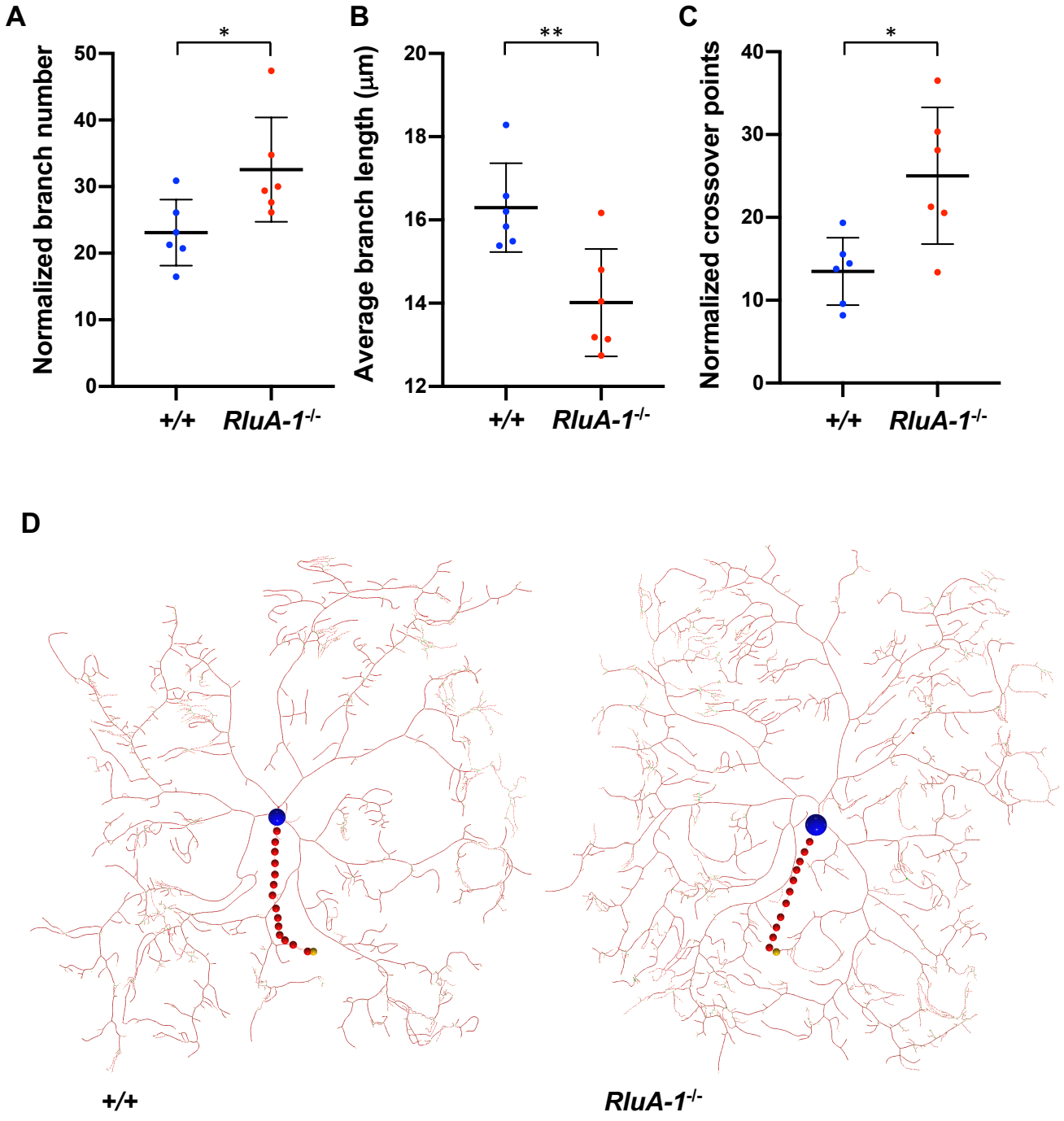
A
Normalized branch number
50
40
30
20
10
0
*
+/+
RluA-1-/-
B
Average branch length (μm)
20
18
16
14
12
**
+/+
RluA-1-/-
C
Normalized crossover points
40
30
20
10
0
*
+/+
RluA-1-/-
D
+/+
RluA-1-/-

Figure 7